

---

# Learning INR for Event-guided Rolling Shutter Frame Correction, Deblur, and Interpolation

---

Yunfan Lu<sup>1</sup>\* Guoqiang Liang<sup>1</sup>\* Lin Wang<sup>1,2</sup>

<sup>1</sup>AI Thrust, HKUST(GZ) <sup>2</sup>Dept. of Computer Science and Engineering, HKUST  
{ylu066, gliang041}@connect.hkust-gz.edu.cn, linwang@ust.hk

## Abstract

Images captured by rolling shutter (RS) cameras under fast camera motion often contain obvious image distortions and blur, which can be modeled as a row-wise combination of a sequence of global shutter (GS) frames within the exposure time. Naturally, recovering high-frame-rate GS sharp frames from an RS blur image needs to simultaneously consider RS correction, deblur, and frame interpolation. Tackling this task is nontrivial, and to our knowledge, no feasible solutions exist by far. A naive way is to decompose the whole process into separate tasks and simply cascade existing methods; however, this results in cumulative errors and noticeable artifacts. Event cameras enjoy many advantages, *e.g.*, high temporal resolution, making them potential for our problem. To this end, we make the **first** attempt to recover high-frame-rate sharp GS frames from an RS blur image and paired event data. Our key idea is *to learn an implicit neural representation (INR) to directly map the position and time coordinates to RGB values to address the interlocking degradations in the image restoration process*. Specifically, we introduce spatial-temporal implicit encoding (STE) to convert an RS blur image and events into a spatial-temporal representation (STR). To query a specific sharp frame (GS or RS), we embed the exposure time into STR and decode the embedded features to recover a sharp frame. Moreover, we propose an RS blur image-guided integral loss to better train the network. Our method is relatively lightweight as it contains only 0.379M parameters and demonstrates high efficiency as the STE is called only once for any number of interpolation frames. Extensive experiments show that our method significantly outperforms prior methods addressing only one or two of the tasks.

## 1 Introduction

Most consumer-level cameras based on CMOS sensors rely on a rolling shutter (RS) mechanism. These cameras dominate the market owing to their benefits, such as low power consumption [11]. In contrast to the global shutter (GS) cameras, RS cameras capture pixels row by row; therefore, the captured images often suffer from obvious spatial distortions (*e.g.*, jitter, stretch) and blur under fast camera/scene motion. And it has been shown that naively neglecting the RS effect often hampers the performance in many real-world applications [10; 15; 44; 45]. In theory, an RS image can be formulated as a row-wise combination of sequential GS frames within the exposure time [4; 5].

In this regard, it is meaningful to *recover high-frame-rate sharp GS frames from a single RS blur image* as the restored high-frame-rate sharp GS frames can directly facilitate many downstream tasks in practice. Intuitively, achieving this goal often needs to simultaneously consider RS correction, deblurring, and frame interpolation. However, tackling this task is nontrivial because multiple

---

\*These authors are co-first authors.

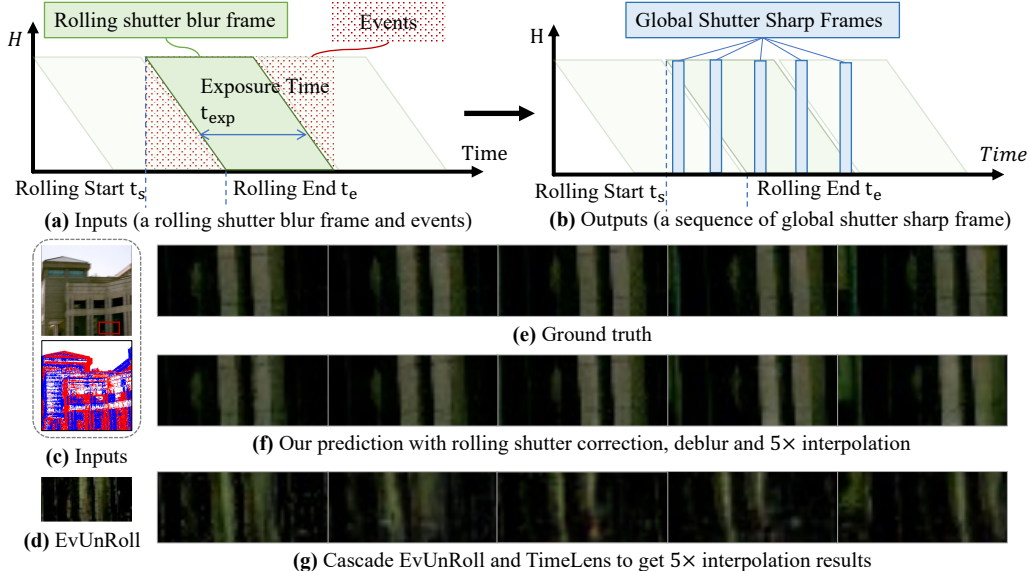


Figure 1: Inputs and the outputs of our method. Inputs are shown in (a), which includes an RS blur image and events.  $t_s$  and  $t_e$  are the start and end timestamps of RS, and  $t_{exp}$  is the exposure time. Outputs are shown in (b), which is a sequence of GS sharp frames during the exposure time.

degradations, such as RS distortion and motion blur, and temporal discontinuity [19; 31], often co-exist for CMOS cameras [44]. The co-existence of various image degradations complicates the whole GS frame restoration process. To the best of our knowledge, no practical solutions exist in the literature to date. A naive way is to decompose the whole process as separate tasks and simply cascading existing image enhancement networks can result in cumulative errors and noticeable artifacts. For example, a simple consideration of cascading a frame interpolation network [1] with RS correction network produces degraded results, as previously verified in [24].

Event cameras offer several advantages, such as high-temporal resolution, which make them suitable for various image restoration tasks [36; 45; 34; 29; 30]. eSL-Net [36] proposes an event-guided sparse learning framework to simultaneously achieve image super-resolution, denoising, and deblurring. TimeLens [34] integrates a synthesis-based branch with a warp-based branch to boost the performance of the video frame interpolation. DeblurSR [29] and E-CIR [30] take advantage of the high temporal resolution of events by converting a blurry frame into a time-to-intensity function, using spike representation and Lagrange polynomials, respectively. EvUnRoll [45] leverages events as guidance to enhance RS correction by accounting for nonlinear motion during the desired timestamp. However, these methods focus on either deblurring or RS correction and can not recover high-frame-rate sharp GS frames from a single RS blur image. An example is depicted in Fig. 1(g), showing that simply cascading event-guided RS correction model (e.g., EvUnroll [45]) and interpolation model (e.g., TimeLens [34]) to recover high-frame-rate sharp GS frames results in obvious artifacts.

In this paper, we make the **first** attempt to propose a novel yet efficient learning framework that can recover high-frame-rate sharp GS frames from an RS blur image, guided by event data. Our key idea is to learn an *implicit neural representation (INR)* to directly map the position and time coordinates to RGB values to address the co-existence of degradations in the image restoration process. This makes it possible to exploit the spatial-temporal relationships from the inputs to achieve RS correction, deblur, and interpolation simultaneously. One distinct advantage of our method is that it is relatively lightweight with only **0.379M** parameters. We formulate the task—recovering high-frame-rate sharp GS frames from an RS blur image and paired event data—as a novel *estimation* problem, defined as a function,  $F(x, t, \theta)$ . Here,  $x$  denotes the pixel position  $(x, y)$  of an image,  $t$  denotes the timestamp during the exposure time, and  $\theta$  denotes the function’s parameters. Our proposed framework consists of three parts: spatial-temporal implicit encoding (STE), exposure time embedding (ETE), and pixel-by-pixel decoding (PPD). Specifically, STE first utilizes sparse learning-based techniques [36] to extract a spatial-temporal representation (STR)  $\theta$  from events and an RS blur image (Sec. 3.2.1). To query a specific sharp frame of RS or GS pattern, we then model

the exposure information as a temporal tensor  $T$  in ETE (Sec. 3.2.2). Finally, PPD leverages an MLP to decode sharp frames from the STR and the temporal tensor  $T$  (Sec. 3.2.3), allowing for the generation of a sharp frame at any given exposure pattern (e.g., RS or GS). One notable advantage of our approach is its high efficiency, as it only requires using the STE once, regardless of the number of interpolation frames. In addition, we introduce the blur frame-guided integral loss from the integral perspective. Such a design makes it better to effectively constrain our network training.

We conduct a thorough evaluation of our proposed method, including both quantitative and qualitative analyses, using a higher resolution ( $256 \times 256$ ) dataset than that of the previous methods ( $180 \times 240$ ) [29; 30]. Extensive experimental results demonstrate that our approach outperforms existing methods in RS correction, deblur, and interpolation (An example can be found in Fig. 1(g)).

## 2 Related Works

### 2.1 Event-guided Image/Video Restoration

**Event-guided Deblurring** Owing to the high temporal resolution afforded by events, prior studies [33; 36; 27; 12] have incorporated events into the task of deblurring. These works focus on the reconstruction of a single GS sharp frame from the GS blur frame, guided by event data. The work most analogous to ours is EvUnroll[45], which first leverages event cameras for RS correction, leveraging their low latency benefits. Nonetheless, EvUnroll primarily focuses on RS correction, with its optional deblurring module equipped to handle only minor motion blur, as illustrated in Fig. 1 (d).

**Event-guided Deblurring + Interpolation** These studies can be bifurcated based on the quantity of input GS blur frames: single GS frame [41; 30; 29; 9] or multiple GS frames [25; 43; 16]. The former, such as E-CIR [30] and DeblurSR [29], convert a GS blur frame into a time-to-intensity function while the latter, e.g., EDI [25], LEDVDI [16], and EVDI [43] are both built upon the event-based double integral model [25]. However, these methods primarily target GS frames affected by motion blur, leading to performance degradation when dealing with spatially distorted and RS blur frames.

### 2.2 Frame-based Video Restoration for RS Inputs

**RS Correction + Interpolation** RSSR [4; 5] is the first work that generates multiple GS frames from two consecutive RS frames by introducing bi-directional undistortion flows. CVR [6] estimates two latent GS frames from two consecutive RS frames, followed by motion enhancement and contextual aggregation before generating final GS frames.

**RS Correction + Deblurring** JCD [44] proposes the first pipeline that employs warping and deblurring branches to effectively address the RS distortion and motion blur. However, JCD’s motion estimation module, built upon the assumption of linear motion derived from DeepUnrollNet [17], encounters a significant performance degradation in real-world scenarios involving non-linear motion [45]. To eliminate the dependence of motion estimation, [38] proposes a method that turns the RS correction into a rectification problem, which allows all pixels to start exposure simultaneously and end exposure line by line. *Differently, our method can recover arbitrary GS sharp frames during the exposure time of RS blur frames without the assumption of linear motion.*

### 2.3 Implicit Neural Representation (INR)

INR [40; 28; 2; 3; 18] is proposed for parameterized signals (images, video or audio) in the coordinate-based representation, inspiring some researchers to explore the potential of INR in low-level vision tasks. LIIF [2] represents images as high-dimensional tensors and allows for upsampling at any scale through interpolation and decoding, followed by VideoINR [3], which extends LIIF to videos, enabling temporal and spatial upsampling at any scale. EG-VSR [18] incorporates events into the learning of INR to achieve random-scale video super-resolution. *Differently, we propose STE to directly map the position and time coordinates to RGB values to address the co-existence of degradations in the image restoration process. Our STE makes it possible to exploit the spatial-temporal relationships from the inputs to achieve RS correction, deblur, and interpolation simultaneously.*

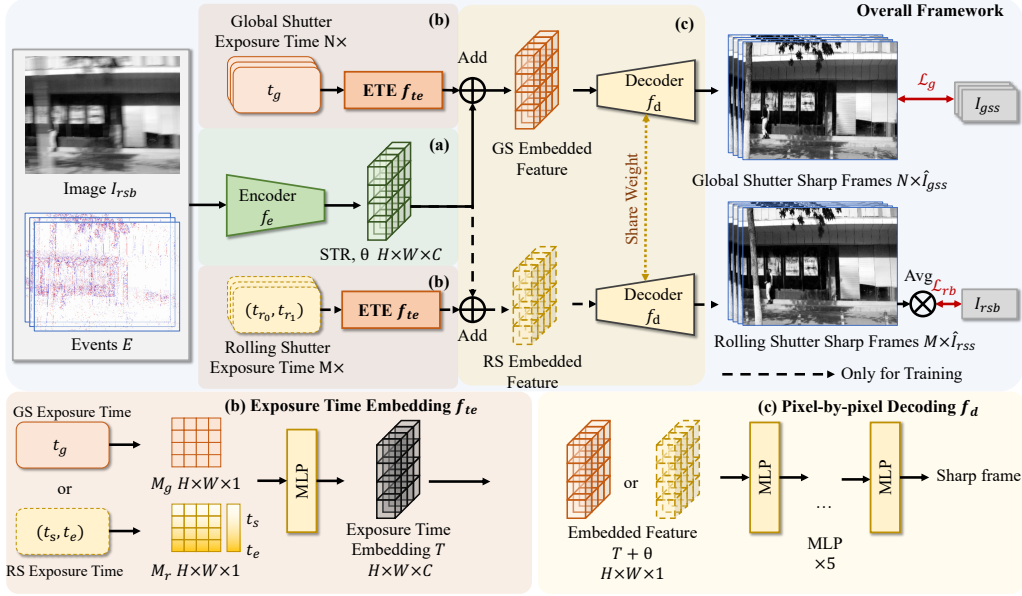


Figure 2: An overview of our framework. Our method consists of three parts, (a) the Spatial-Temporal Implicit Encoding (STE), (b) Exposure Time Embedding (ETE), and (c) Pixel-by-pixel decoding (PPD). Details of STE, ETE, and PPD are described in Sec. 3.2.1, Sec. 3.2.2, and Sec. 3.2.3. The inputs are an RS blur image  $I_{rsb}$  and events, and the outputs are a sequence of GS frames and RS frames. RS frames are predicted only in training.

### 3 Methodology

#### 3.1 Problem Definition and Analysis

We formulate the task —*recovering high-frame-rate sharp GS frames from an RS blur image and paired event data*— as a novel estimation problem, defined as a function,  $F(\mathbf{x}, t, \theta)$ . Here,  $\mathbf{x}$  denotes the pixel position  $(x, y)$  of an image with a resolution of  $H \times W$ ,  $t$  denotes the timestamp during the exposure time, and  $\theta$  denotes the parameters. The intuition behind this formulation is that there exists a relationship between the RS blur/sharp frame and the GS blur/sharp frame. We now describe it. By defining a function  $F(\mathbf{x}, t, \theta)$  mapping the pixel position  $\mathbf{x} = (x, y)$  and timestamp  $t$  to intensity or RGB value, we can obtain a GS sharp frame by inputting the desired timestamp  $\hat{t}$  during the exposure time to the function, which can be formulated as  $I_{g, \hat{t}} = F(\mathbf{x}, \hat{t}, \theta)$ . As an RS image can be formulated as a row-wise combination of sequential GS frames within the exposure time [4; 5], we can assemble an RS sharp frame  $I_{r, t_s, t_e}$  from a sequence of GS sharp frames row by row given the RS start time  $t_s$  and the end time  $t_e$ . In other words, the  $h$ -th row of an RS frame is the same as the  $h$ -th row of a GS frame at  $t_s^h$ , and the exposure start timestamp of the  $h$ -th row of an RS frame is  $t_s^h = t_s + h \times (t_e - t_s)/H$ . Therefore, we can formally describe an RS sharp frame as follows:

$$I_{r, t_s, t_e} = \{F(\mathbf{x}, t_s^h, \theta)[h], h \in [0, H]\}. \quad (1)$$

In principle, a blur frame can be regarded as the temporal average of a sequence of sharp frames [23; 42]. Thus, a GS blur frame  $I_{g, t_g, t_{exp}}$ , where  $t_g$  is the exposure start timestamp and  $t_{exp}$  is the exposure time, can be expressed as the average of a sequence of GS sharp frames during the exposure time  $t_{exp}$ , which can be formulated as:

$$I_{g, t_g, t_{exp}} = \frac{1}{t_{exp}} \int_{t_g}^{t_g + t_{exp}} F(\mathbf{x}, t, \theta) dt \approx \frac{1}{N} \sum_{i=0}^{N-1} I_{g, t_g + i \times t_{exp}/N}, \quad (2)$$

where  $N$  is the length of the GS frame sequence.

With above formulation, an RS blur frame  $I_{r, t_s \rightarrow t_e, t_{exp}}$  can thus be described based on the RS start time  $t_s$ , RS end time  $t_e$ , and exposure time of each scan line  $t_{exp}$ , as depicted in Fig. 1 (a). According

to Eq. 1 and Eq. 2, the  $h$ -th row of an RS blur frame can be described as the temporal average of the  $h$ -th row in a sequence of GS sharp frames, which can be written as follows:

$$I_{r,t_s \rightarrow t_e,t_{exp}} = \left\{ \frac{1}{t_{exp}} \int_{t_s}^{t_s+t_{exp}} F(\mathbf{x}, t_s + \frac{h}{H} \times (t_e - t_s), \theta) [h] dt, h \in [0, H] \right\} \quad (3)$$

$$\approx \left\{ \frac{1}{N} \sum_{i=0}^N I_{g,t_s+i \times t_{exp}/N} [h], h \in [0, H] \right\}.$$

An event stream  $E$  consists of a set of event  $e = (x, y, t, p)$ , where each event is triggered and recorded with the polarity  $p$  when the logarithmic brightness change at pixel  $(x, y)$  exceeds a certain threshold  $C$ , which can be approximated as the differential of  $F(\mathbf{x}, t, \theta)$  with respect to the time dimension. *For details about the principle of event cameras, refer to the supplementary material.*

To use event data  $E$  as guidance, we need to address three challenges to estimate the mapping function  $F(\mathbf{x}, t, \theta)$ : **1**) how to find a function  $f_e$  to encode the input RS blur image and events to  $\theta$  of the mapping function  $F(\mathbf{x}, t, \theta)$ ; **2**) how to find a function  $f_{te}$  to represent the exposure information of desired RS or GS sharp frames as  $t$  of the mapping function  $F(\mathbf{x}, t, \theta)$ ; **3**) how to find a function  $f_d$  to eliminate the need to input position information of desired RS or GS sharp frames as  $p$  of the mapping function  $F(\mathbf{x}, t, \theta)$ . Therefore, our goal is to estimate  $f_e$ ,  $f_{te}$ , and  $f_d$  in order to get a mapped result, which can be formulated as:

$$I = F(\mathbf{x}, t, \theta) = F(\mathbf{x}, t, f_e(E, I_{rsb})) = F(\mathbf{x}, f_{te}(t), f_e(E, I_{rsb})) = f_d(f_{te}(t), f_e(E, I_{rsb})). \quad (4)$$

In the following section, we describe our framework based on Eq. 4 by substantiating  $f_e$ ,  $f_{te}$ , and  $f_d$ .

## 3.2 Proposed Framework

An overview of our framework is depicted in Fig. 2, which takes an RS blur image  $I_{rsb}$  and paired events  $E$  as inputs and outputs  $N$  sharp GS frames  $\{I_{gss}\}_{i=0}^N$  with a high-frame-rate. To substantiate the defined functions  $f_e$ ,  $f_{te}$ , and  $f_d$ , as mentioned in Sec. 3.1, our proposed framework consists of three components: **1**) Spatial-Temporal Implicit Encoding (STE), **2**) Exposure Time Embedding (ETE), and **3**) Pixel-by-pixel Decoding (PPD). Specifically, we first introduce an STE with deformable convolution [37] to encode the RS blur frame and events into a spatial-temporal representation (STR) (Sec. 3.2.1). To provide exposure temporal information for STR, we embed the exposure start timestamp of each pixel from the GS or RS by ETE. (Sec. 3.2.2). Lastly, the PPD module adds ETE to STR to generate RS or GS sharp frames (Sec. 3.2.3). We now describe these components in detail.

### 3.2.1 Spatial-Temporal Implicit Encoding (STE)

Based on the analysis in Sec. 3.1, we conclude that the RS blur frame  $I_{rsb}$  and events  $E$  collectively encompass the comprehensive spatial-temporal information during the exposure process. In this section, we aim to extract a spatial-temporal implicit representation  $\theta$  that can effectively capture the spatial-temporal information from the RS blur frame  $I_{rsb}$  and events  $E$ .

To achieve this, we need to consider two key factors: (1) extracting features for the multi-task purpose and (2) estimating motion information. For the first factor, we draw inspiration from eSL-Net [36], which effectively utilizes events to simultaneously handle deblur, denoise, and super-resolution tasks. Accordingly, we design a sparse-learning-based backbone for the encoder. Regarding the second factor, in previous works, the optical flow has been commonly used for motion estimation in RS correction and interpolation tasks [4; 6; 5]. However, optical flow estimation is computationally demanding [8; 46; 32], making it challenging to incorporate it into the multiple task framework for RS cameras due to the complex degradation process. As an efficient alternative, we employ deformable convolution [37] in our encoder to replace the optical flow estimation module. We adopt a 3D tensor with a shape of  $H \times W \times C$  as the STR  $\theta$ , which can effectively address the interlocking degradations encountered in the image restoration process with a sparse-learning-based backbone and deformable convolution, as formulated as  $\theta = f_e(E, I_{rsb})$  in Eq. 4. *For more details regarding the encoding network structure, please refer to the supplementary material.*

### 3.2.2 Exposure Time Embedding (ETE)

As depicted in Fig. 2 (b), the primary objective of the ETE module is to incorporate the exposure time of either a rolling shutter (RS) frame  $(t_s, t_e)$  or a global shutter (GS) frame  $(t_g)$  by employing an MLP layer, resulting in the generation of a temporal tensor  $T$ . To achieve this, we design an ETE

module, denoted as  $f_{te}$ , which takes the GS exposure time  $t_g$  as input and produces the GS temporal tensor  $T_g = f_{te}(t_g)$ . Similarly, for RS frames,  $T_r = f_{te}(t_{r_s}, t_{r_e})$  represents the RS temporal tensor, which is only used in training. The process begins by converting the exposure process information into a timestamp map, with a shape of  $H \times W \times 1$ . Subsequently, the timestamp map is embedded by increasing its dimensionality to match the shape of the STR. This embedding procedure allows for the integration of the exposure time information into the STR representation. We now explain the construction of timestamp maps for both GS and RS frames and describe the embedding method employed in our approach.

**GS Timestamp Map:** In GS sharp frames, all pixels are exposed simultaneously, resulting in the same exposure timestamps for pixels in different positions. Given a GS exposure timestamp  $t_g$ , the GS timestamp map  $M_g$  can be represented as  $M_g[h][w] = t_g$ , where  $h$  and  $w$  denote the row and column indices, respectively.

**RS Timestamp Map:** According to the analysis in Sec. 3.1, pixels in RS frames are exposed line by line, and pixels in different rows have different exposure start timestamps. Given RS exposure information with start time  $t_s$  and RS end time  $t_e$ , the RS timestamp map can be represented as  $M_r[h][w] = t_s + (t_e - t_s) \times h/H$ , where  $h, w, H$  denote the row and column indices and height of the image, respectively.

**Time Embedding:** The timestamp maps,  $M_r$  and  $M_g$ , represent the timestamps of each pixel in a specific frame (RS or GS) with a shape of  $H \times W \times 1$ . However, the timestamp map is a high-frequency variable and can pose challenges for learning neural networks [35]. Some approaches [35; 40] propose a combination function of sine and cosine to encode the positional embedding. Nonetheless, calculating the derivative of the positional embedding is difficult, limiting its practical application to image enhancement tasks. In this paper, we utilize a one-layer MLP to increase the dimension for embedding. The whole embedding process is formulated as  $T_g = f_{te}(t_g)$  for GS frames, and  $T_r = f_{te}(t_{r_s}, t_{r_e})$  for RS frames, as depicted in Fig. 2(b). The MLP consists of a single layer that maps the timestamp map  $M_r$  or  $M_g$  to the same dimension  $H \times W \times C$  as the spatial-temporal representation (STR)  $\theta$ , as described in Sec. 3.2.1.

### 3.2.3 Pixel-by-pixel Decoding (PPD)

As shown in Fig. 2 (c), the goal of PPD is to efficiently query a sharp frame from STR  $\theta$  by the temporal tensor  $T$ . It is important that the encoder is invoked only once for  $N$  times interpolation, while the decoder is called  $N$  times. Therefore, the efficiency of this query is crucial for the overall performance. The query’s inputs  $\theta$  capture the global spatial-temporal information, and  $T$  captures the temporal information of the sharp frame (GS or RS). Inspired by previous works [21; 2], we directly incorporate the temporal tensor  $T$  into the STR  $\theta$  to obtain an embedded feature with a shape of  $H \times W \times C$  for each query. This additional embedded feature combines the global spatial-temporal information with the local exposure information, enabling straightforward decoding to obtain a sharp frame. To avoid the need for explicit positional queries, we employ a pixel-by-pixel decoder. The decoder, denoted as  $f_d$  in Eq. 4, employs a simple 5-layer MLP  $f_{mlp}^{\odot 5}$  architecture. The reconstructed output  $I$  after decoding can be described in Eq. 5, where  $\oplus$  means element-wise addition.

$$I = f_d(f_{te}(t), f_e(E, I_{rsb})) = f_d(T, \theta) = f_{mlp}^{\odot 5}(T \oplus \theta). \quad (5)$$

### 3.2.4 Loss Function

**RS Blur Image-guided Integral Loss:** Inspired by EVDI [43], we formulate the relationship between RS blur frames and RS sharp frames. Given a sequence of RS sharp frames generated from the decoder, the input RS blur frame  $I_{rsb}$  can be reconstructed as Eq. 6, where  $M$  represents the length of the RS image sequence and  $\gamma$  represents the CRF function [22]. In this way, we can formulate the blur frame guidance integral loss between the reconstructed RS blur frame and the original RS blur frame as  $\mathcal{L}_b = \mathcal{L}_c(\hat{I}_{rsb}, I_{rsb})$ , where  $\mathcal{L}_c$  indicates *Charbonnier loss* [14].

$$\hat{I}_{rsb} \approx \frac{1}{M} \left( \sum_{i=1}^M (\hat{I}_{r_{ss}}^i)^{1/\gamma} \right)^\gamma. \quad (6)$$

**Total Loss:** Apart from RS blur image-guided integral loss  $\mathcal{L}_b$ , we incorporate a reconstruction loss  $\mathcal{L}_{r_e}$  to supervise the reconstructed GS sharp frames. Our method consists of two losses: RS blur

image-guided integral loss and the reconstruction loss, where  $\lambda_b, \lambda_{re}$  denote the weights of each loss:

$$\mathcal{L} = \lambda_b \mathcal{L}_b + \lambda_{re} \mathcal{L}_{re} = \lambda_b \mathcal{L}_c(\hat{I}_{rsb}, I_{rsb}) + \lambda_{re} \frac{1}{N} \sum_{k=1}^N \mathcal{L}_c(\hat{I}_{gss}^k, I_{gss}^k). \quad (7)$$

## 4 Experiments

**Implementation Details:** We utilize the Adam optimizer [13] for all experiments, with learning rates of  $1e-4$  for both Gev-RS [45] and Fastec-RS [17] datasets. PSNR and SSIM [39] are used to evaluate the reconstructed results.

**Datasets: 1) Gev-RS dataset** [45] contains original videos shot by GS high-speed cameras with  $1280 \times 720$  resolution at 5700 fps. However, EvUnroll [45] primarily focuses on RS correction, and provided by EvUnroll Gev-RS dataset does not include RS frames with severe motion blur. Therefore, we reconstruct RS frames with severe motion blur and events from original videos. We initially downsample the original videos to DAVIS346 event camera’s resolution ( $260 \times 346$ ) [26]. Then, we employ the event simulator vid2e [7] to synthesize events from the resized frames. We simulate RS blur frames by first generating RS sharp frames as the same RS simulation process of Fastec-RS [17] and then averaging 260 RS sharp frames after gamma correction. We use the same dataset split as EvUnroll [45], with 20 videos used for training and 9 videos used for testing. **2) Fastec-RS dataset** [17] provides the original frame sequences recorded by the high-speed GS cameras with the resolution of  $640 \times 480$  at 2400 fps. We use the same settings to resize frame sequences, create events, and RS blurry frames. Furthermore, we use the same dataset split strategy as Fastec-RS [17]: 56 sequences for training and 20 sequences for testing.

### 4.1 Comparison with SOTA methods

We compare our method with recent methods with two different settings on Gev-RS [45] and Fastec-RS [17] datasets: **(I)** the experiment with a single GS sharp frame result, which includes JCD [44] (frame-based RS correction and deblurring), EvUnroll [45] (event-guided RS correction), and eSL-Net [36] (event-guided deblurring). **(II)** the experiment with a sequence of GS sharp frames result, which includes DeblurSR [29] (event-guided deblurring and interpolation), and the combination of EvUnroll [45] and TimeLens [34] (event-guided video frame interpolation). We evaluate JCD, EvUnroll, TimeLens, and DeblurSR with the released code. We modified eSL-Net by adjusting its parameterization initialization method and removing the up-sampling module, allowing it to be well-trained on our datasets. The outputs of eSL-Net and DeblurSR are grayscale frames, and the outputs of JCD, EvUnroll, and the combination of EvUnroll and TimeLens are RGB frames. For fairness, our network is trained with the input of grayscale and RGB images, respectively. The quantitative results for experiments generating a single GS sharp frame ( $1\times$ ) and those producing a sequence of GS sharp frames ( $3\times, 5\times, 9\times$ ) are presented in Tab. 1. In comparison to methods that yield a single GS sharp frame, our approach exhibits remarkable performance in both grayscale and RGB frames, surpassing the best-performing methods (eSL-Net [36] in grayscale and EvUnroll [45] in RGB) by **1.48dB** and **4.17dB** on the Gev-RS [45] dataset, respectively. In scenarios where a sequence of GS sharp frames is produced, our method attains optimal performance for both grayscale and RGB frames, achieving an increase of up to **13.47dB** and **8.49dB** compared to DeblurSR [29] and EvUnroll [45]+TimeLens [34] on the Gev-RS [45] dataset, respectively. The substantial performance decline of DeblurSR [29] can be ascribed to the interdependence between RS correction and deblur. The performance reduction of EvUnroll+TimeLens can be accounted for by the accumulation of errors arising from this cascading network, as depicted in Fig. 1 (g).

The qualitative results, as depicted in Fig. 3, showcase the effectiveness of our proposed method on both grayscale and RGB inputs. These results serve to demonstrate the ability of our approach to generate sharp frames devoid of RS distortion, thereby yielding the most visually pleasing outcomes in challenging scenarios involving a fast-moving train with motion blur and RS distortion. Comparatively, the results of eSL-Net and EvUnroll exhibit discernible noise, particularly evident around the train door within the red region of Fig. 3. Another approach, JCD, falls short in recovering sharp frames within such complex scenes. This failure can be attributed to the insufficient availability of frame-based methods which rely on the assumption of linear motion. Furthermore, the results obtained using DeblurSR [29] display noticeable artifacts, particularly in the context of the moving train. These artifacts hinder satisfactory frame reconstruction in such dynamic environments.

Table 1: Quantitative results for RS correction, deblurring, and frame interpolation. G, C, and E represent the grayscale frame, color frame, and events. TL refers to TimeLens [34] and EU refers to EvUnroll [45].

Methods	Inputs	Params(M)	Gev-RS		Fastec-RS			
			PSNR	SSIM	PSNR	SSIM		
1×	eSL-Net (modified) [36]	1 G+E	0.1360		31.64	0.9614	32.45	0.9186
	Ours (gray)	1 G+E	0.3790		<b>33.12</b>	<b>0.9881</b>	<b>34.62</b>	<b>0.9390</b>
	JCD [44]	3 C	7.1659		18.59	0.5781	21.31	0.6150
	EU [45]	1 C+E	20.83		26.18	0.8606	29.76	0.8693
	Ours (color)	1 C+E	0.3792		<b>30.35</b>	<b>0.9714</b>	<b>33.64</b>	<b>0.9299</b>
3×	DeblurSR [29]	1 G+E	21.2954		17.64	0.554	21.17	0.5816
	Ours (gray)	1 G+E	0.3790		<b>31.11</b>	<b>0.9738</b>	<b>33.23</b>	<b>0.9210</b>
	EU [45] + TL [34]	2 C+E	93.03		21.86	0.7057	24.81	0.7179
	Ours (color)	1 C+E	0.3792		<b>30.35</b>	<b>0.9714</b>	<b>32.72</b>	<b>0.9147</b>
5×	DeblurSR [29]	1 G+E	21.2954		18.35	0.6107	22.86	0.6562
	Ours (gray)	1 G+E	0.3790		<b>30.84</b>	<b>0.9673</b>	<b>32.82</b>	<b>0.9147</b>
	EU [45] + TL [34]	2 C+E	93.03		21.59	0.6964	24.46	0.7140
	Ours (color)	1 C+E	0.3792		<b>28.41</b>	<b>0.9062</b>	<b>32.13</b>	<b>0.9053</b>
9×	DeblurSR [29]	1 G+E	21.2954		18.86	0.6502	23.96	0.7049
	Ours (gray)	1 G+E	0.3790		<b>30.54</b>	<b>0.9579</b>	<b>32.21</b>	<b>0.9051</b>
	EU [45] + TL [34]	2 C+E	93.03		21.24	0.6869	23.99	0.7029
	Ours (color)	1 C+E	0.3792		<b>27.21</b>	<b>0.8869</b>	<b>29.31</b>	<b>0.8590</b>

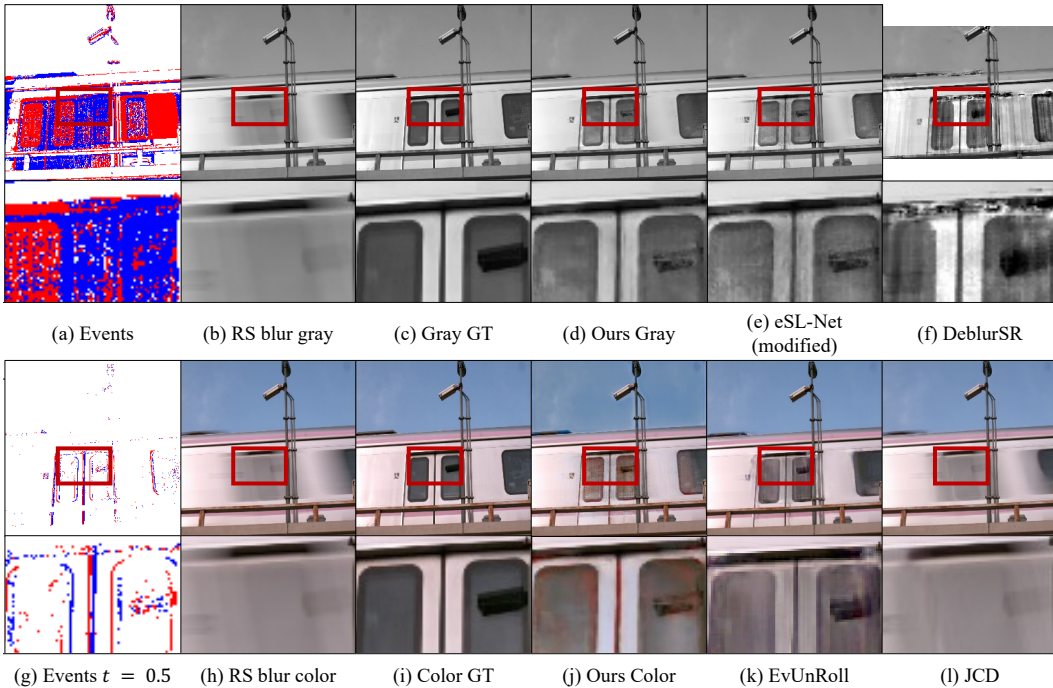


Figure 3: Visual Comparisons on RS correction and deblurring on Gev-RS [45] dataset. The image resolution of DeblurSR [29] is  $180 \times 240$ .

## 4.2 Ablation and Analytical Studies

**Importance of Exposure Time Embedding:** We conduct the experiments to evaluate the impact of learning-based position embedding, with a comparative analysis to sinusoid position embedding [35]. As indicated in Tab. 2, learning-based position embedding outperforms sinusoid position embedding across all interpolation conditions, with advancements of up to **0.66dB**. This superior efficacy is attributable to the intrinsic adaptability of the learning-based position embedding.



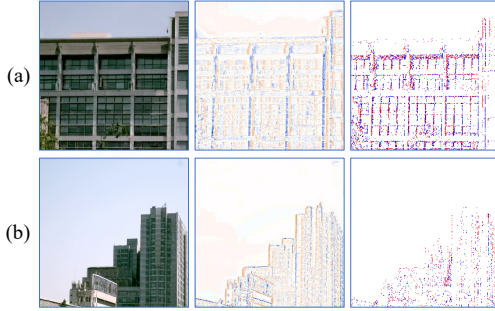


Figure 4: (a) and (b) are two different scenes. From left to right: the predicted images, temporal gradients ( $\partial F(\mathbf{x}, t, \theta)/\partial t$ ), and events. Orange and blue hues in the image signify positive and negative gradients, respectively. The color intensity is associated with the gradient value, with higher absolute values manifested by stronger colors.

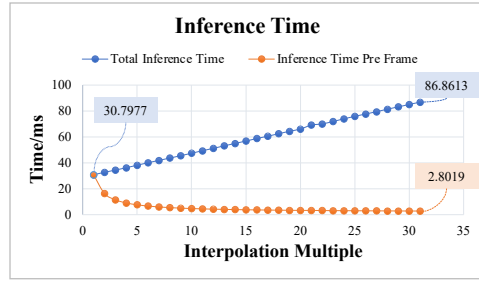


Figure 5: The illustration of inference time of our method. The horizontal axis represents the frame interpolation multiple, while the vertical axis represents the time. The blue line represents the total inference time, while the yellow line represents the average time per frame. The interpolation multiple ranges from  $1\times$  to  $31\times$ .

**Visualization of Temporal Dimension Gradients:** Fig. 4 depicts the visualization of the gradients in the temporal dimension, demonstrating the successful training of the function  $F(\mathbf{x}, t, \theta)$ . Both the gradient visualization and events exhibit a similar intensity trend for  $F(\mathbf{x}, t, \theta)$  at the specified time  $t$ . However, the gradient visualization appears smoother with more continuous edges. This observation confirms that our method is capable of learning the high temporal resolution of intensity changes present in events, simultaneously filtering out noise.

**Importance of RS Blur Image-guided Integral Loss:** The effectiveness of the RS blur image-guided integral Loss across diverse interpolation settings is depicted in Tab. 3. The findings point towards the enhancement in PSNR for high interpolation configurations (*e.g.*,  $9\times$ ) upon employing this loss.

The enhancement observed can be attributed to the increased number of RS sharp frames provided by higher interpolation settings. This increased supply to the integral operation ensures that the reconstructed RS blur frames bear a greater resemblance to the input RS blur frames

**Inference Speed:** Fig. 5 illustrates the inference time of our method with a wide range of interpolation multiples spanning from  $1\times$  to  $31\times$ , including the total inference time and the average inference time per frame. Importantly, the total inference time increases gradually as the frame interpolation multiple increases. For instance, when going from  $1\times$  frame interpolation to  $31\times$  frame interpolation, the total inference time only increases from  $30.8\text{ ms}$  to  $86.9\text{ ms}$ . This signifies a mere 2.8-fold increase in time despite a 31-fold increase in the interpolation multiple. Additionally, it is notable that the average inference time per frame decreases with higher frame interpolation multiples. At  $31\times$  frame interpolation, the average time per frame is a mere  $2.8\text{ ms}$ .

Table 2: Ablation for learning-based position embedding.

	Position Embedding	PSNR	SSIM
$1\times$	Sinusoid	32.46	0.9851
	Learning	<b>33.12</b>	<b>0.9881</b>
$3\times$	Sinusoid	30.83	0.9723
	Learning	<b>31.11</b>	<b>0.9738</b>
$5\times$	Sinusoid	30.70	0.9678
	Learning	<b>30.84</b>	<b>0.9673</b>
$9\times$	Sinusoid	30.51	0.9560
	Learning	<b>30.54</b>	<b>0.9579</b>

Table 3: Ablation for the loss function.

	$\mathcal{L}_b$	PSNR	SSIM
$1\times$	✗	33.12	0.9881
	✓	33.14	0.9844
$3\times$	✗	31.11	0.9738
	✓	31.09	0.9768
$5\times$	✗	30.84	0.9673
	✓	30.83	0.9784
$9\times$	✗	30.54	0.9579
	✓	30.61	0.9538

It is important to note that other methods, *e.g.*, EvUnRoll [45] + TimeLens [34], involve additional I/O operations during inference. Specifically, the output of EvUnRoll needs to be stored and then read by TimeLens, resulting in significantly longer inference times. Additionally, the DeblurSR [29] input has a lower resolution ( $180\times 240$ ) compared to our method ( $256\times 256$ ). Moreover, our method leverages mixed precision technology [20] during inference, a capability that was not utilized in the

forementioned methods. Therefore, we conducted a numerical analysis exclusively on the inference time of our proposed method, given its clear advantage in inference speed.

## 5 Conclusion

This paper presented a novel approach that simultaneously uses events to guide rolling shutter frame correction, deblur, and interpolation. Unlike previous network structures that can only address one or two image enhancement tasks, our method incorporated all three tasks concurrently, providing potential for future expansion into areas such as image and video super-resolution and denoising. Furthermore, our approach demonstrated high efficiency in computational complexity and model size. Regardless of the number of frames involved in interpolation, our method only requires a single call to the encoder, and the model size is a mere 0.37M.

**Limitations** The experimental data used in our analysis is based on simulation data and lacks real-world data. Collecting real data is a challenging task, but in future research, we intend to address this limitation by employing optical devices like spectroscopes to gather real-world data.

**Broader Impact** The method proposed herein provides a concurrent solution for the guidance of RS frame correction, deblurring, and interpolation, leveraging event-based data. Through the utilization of INR, these three tasks are executed effectively in unison by our method. Furthermore, the notable efficiency of our approach paves the way for the application of event-guided image enhancement in a multitude of contexts, inclusive of mobile drive scenarios.

## References

- [1] Wenbo Bao, Wei-Sheng Lai, Chao Ma, Xiaoyun Zhang, Zhiyong Gao, and Ming-Hsuan Yang. Depth-aware video frame interpolation. In *Proceedings of the IEEE/CVF Conference on Computer Vision and Pattern Recognition*, pages 3703–3712, 2019. 2
- [2] Yinbo Chen, Sifei Liu, and Xiaolong Wang. Learning continuous image representation with local implicit image function. In *Proceedings of the IEEE/CVF conference on computer vision and pattern recognition*, pages 8628–8638, 2021. 3, 6
- [3] Zeyuan Chen, Yinbo Chen, Jingwen Liu, Xingqian Xu, Vidit Goel, Zhangyang Wang, Humphrey Shi, and Xiaolong Wang. Videoinr: Learning video implicit neural representation for continuous space-time super-resolution. In *Proceedings of the IEEE/CVF Conference on Computer Vision and Pattern Recognition*, pages 2047–2057, 2022. 3
- [4] Bin Fan and Yuchao Dai. Inverting a rolling shutter camera: bring rolling shutter images to high framerate global shutter video. In *Proceedings of the IEEE/CVF International Conference on Computer Vision*, pages 4228–4237, 2021. 1, 3, 4, 5
- [5] Bin Fan, Yuchao Dai, and Hongdong Li. Rolling shutter inversion: Bring rolling shutter images to high framerate global shutter video. *IEEE Transactions on Pattern Analysis & Machine Intelligence*, 45(05):6214–6230, 2023. 1, 3, 4, 5
- [6] Bin Fan, Yuchao Dai, Zhiyuan Zhang, Qi Liu, and Mingyi He. Context-aware video reconstruction for rolling shutter cameras. In *Proceedings of the IEEE/CVF Conference on Computer Vision and Pattern Recognition*, pages 17572–17582, 2022. 3, 5
- [7] Daniel Gehrig, Mathias Gehrig, Javier Hidalgo-Carrió, and Davide Scaramuzza. Video to events: Recycling video datasets for event cameras. In *Proceedings of the IEEE/CVF Conference on Computer Vision and Pattern Recognition*, pages 3586–3595, 2020. 7
- [8] Mathias Gehrig, Mario Millhäusler, Daniel Gehrig, and Davide Scaramuzza. E-raft: Dense optical flow from event cameras. In *2021 International Conference on 3D Vision (3DV)*, pages 197–206. IEEE, 2021. 5
- [9] Chen Haoyu, Teng Minggui, Shi Boxin, Wang Yizhou, and Huang Tiejun. Learning to deblur and generate high frame rate video with an event camera. *arXiv preprint arXiv:2003.00847*, 2020. 3
- [10] Johan Hedborg, Per-Erik Forssén, Michael Felsberg, and Erik Ringaby. Rolling shutter bundle adjustment. In *2012 IEEE Conference on Computer Vision and Pattern Recognition*, pages 1434–1441. IEEE, 2012. 1
- [11] James Janesick, Jeff Pinter, Robert Potter, Tom Elliott, James Andrews, John Tower, John Cheng, and Jeanne Bishop. Fundamental performance differences between cmos and ccd imagers: part iii. In *Astronomical and Space Optical Systems*, volume 7439, pages 47–72. SPIE, 2009. 1

- [12] Taewoo Kim, Jeongmin Lee, Lin Wang, and Kuk-Jin Yoon. Event-guided deblurring of unknown exposure time videos. In *Computer Vision–ECCV 2022: 17th European Conference, Tel Aviv, Israel, October 23–27, 2022, Proceedings, Part XVIII*, pages 519–538. Springer, 2022. 3
- [13] Diederik P Kingma and Jimmy Ba. Adam: A method for stochastic optimization. *arXiv preprint arXiv:1412.6980*, 2014. 7
- [14] Wei-Sheng Lai, Jia-Bin Huang, Narendra Ahuja, and Ming-Hsuan Yang. Fast and accurate image super-resolution with deep laplacian pyramid networks. *IEEE transactions on pattern analysis and machine intelligence*, 41(11):2599–2613, 2018. 6
- [15] Yizhen Lao and Omar Ait-Aider. Rolling shutter homography and its applications. *IEEE transactions on pattern analysis and machine intelligence*, 43(8):2780–2793, 2020. 1
- [16] Songnan Lin, Jiawei Zhang, Jinshan Pan, Zhe Jiang, Dongqing Zou, Yongtian Wang, Jing Chen, and Jimmy Ren. Learning event-driven video deblurring and interpolation. In *Computer Vision–ECCV 2020: 16th European Conference, Glasgow, UK, August 23–28, 2020, Proceedings, Part VIII 16*, pages 695–710. Springer, 2020. 3
- [17] Peidong Liu, Zhaopeng Cui, Viktor Larsson, and Marc Pollefeys. Deep shutter unrolling network. In *Proceedings of the IEEE/CVF Conference on Computer Vision and Pattern Recognition*, pages 5941–5949, 2020. 3, 7
- [18] Yunfan Lu, Zipeng Wang, Minjie Liu, Hongjian Wang, and Lin Wang. Learning spatial-temporal implicit neural representations for event-guided video super-resolution. *arXiv preprint arXiv:2303.13767*, 2023. 3
- [19] Maxime Meilland, Tom Drummond, and Andrew I Comport. A unified rolling shutter and motion blur model for 3d visual registration. In *Proceedings of the IEEE International Conference on Computer Vision*, pages 2016–2023, 2013. 2
- [20] Paulius Micikevicius, Sharan Narang, Jonah Alben, Gregory Diamos, Erich Elsen, David Garcia, Boris Ginsburg, Michael Houston, Oleksii Kuchaiev, Ganesh Venkatesh, et al. Mixed precision training. *arXiv preprint arXiv:1710.03740*, 2017. 9
- [21] Ben Mildenhall, Pratul P Srinivasan, Matthew Tancik, Jonathan T Barron, Ravi Ramamoorthi, and Ren Ng. Nerf: Representing scenes as neural radiance fields for view synthesis. *Communications of the ACM*, 65(1):99–106, 2021. 6
- [22] Seungjun Nah, Tae Hyun Kim, and Kyoung Mu Lee. Deep multi-scale convolutional neural network for dynamic scene deblurring. In *Proceedings of the IEEE conference on computer vision and pattern recognition*, pages 3883–3891, 2017. 6
- [23] Seungjun Nah, Tae Hyun Kim, and Kyoung Mu Lee. Deep multi-scale convolutional neural network for dynamic scene deblurring. In *CVPR*, July 2017. 4
- [24] Eyal Naor, Itai Antebi, Shai Bagon, and Michal Irani. Combining internal and external constraints for unrolling shutter in videos. In *Computer Vision–ECCV 2022: 17th European Conference, Tel Aviv, Israel, October 23–27, 2022, Proceedings, Part XVII*, pages 119–134. Springer, 2022. 2
- [25] Liyuan Pan, Cedric Scheerlinck, Xin Yu, Richard Hartley, Miaomiao Liu, and Yuchao Dai. Bringing a blurry frame alive at high frame-rate with an event camera. In *Proceedings of the IEEE/CVF Conference on Computer Vision and Pattern Recognition*, pages 6820–6829, 2019. 3
- [26] Cedric Scheerlinck, Henri Rebecq, Timo Stoffregen, Nick Barnes, Robert Mahony, and Davide Scaramuzza. Ced: Color event camera dataset. In *Proceedings of the IEEE/CVF Conference on Computer Vision and Pattern Recognition Workshops*, pages 0–0, 2019. 7
- [27] Wei Shang, Dongwei Ren, Dongqing Zou, Jimmy S Ren, Ping Luo, and Wangmeng Zuo. Bringing events into video deblurring with non-consecutively blurry frames. In *Proceedings of the IEEE/CVF International Conference on Computer Vision*, pages 4531–4540, 2021. 3
- [28] Vincent Sitzmann, Julien Martel, Alexander Bergman, David Lindell, and Gordon Wetzstein. Implicit neural representations with periodic activation functions. *Advances in Neural Information Processing Systems*, 33:7462–7473, 2020. 3
- [29] Chen Song, Chandrajit Bajaj, and Qixing Huang. Deblursr: Event-based motion deblurring under the spiking representation. *arXiv preprint arXiv:2303.08977*, 2023. 2, 3, 7, 8, 9

- [30] Chen Song, Qixing Huang, and Chandrajit Bajaj. E-cir: Event-enhanced continuous intensity recovery. In *Proceedings of the IEEE/CVF Conference on Computer Vision and Pattern Recognition*, pages 7803–7812, 2022. 2, 3
- [31] Shuochen Su and Wolfgang Heidrich. Rolling shutter motion deblurring. In *Proceedings of the IEEE Conference on Computer Vision and Pattern Recognition*, pages 1529–1537, 2015. 2
- [32] Deqing Sun, Xiaodong Yang, Ming-Yu Liu, and Jan Kautz. Pwc-net: Cnns for optical flow using pyramid, warping, and cost volume. In *Proceedings of the IEEE conference on computer vision and pattern recognition*, pages 8934–8943, 2018. 5
- [33] Lei Sun, Christos Sakaridis, Jingyun Liang, Qi Jiang, Kailun Yang, Peng Sun, Yaozu Ye, Kaiwei Wang, and Luc Van Gool. Event-based fusion for motion deblurring with cross-modal attention. In *Computer Vision–ECCV 2022: 17th European Conference, Tel Aviv, Israel, October 23–27, 2022, Proceedings, Part XVIII*, pages 412–428. Springer, 2022. 3
- [34] Stepan Tulyakov, Daniel Gehrig, Stamatis Georgoulis, Julius Erbach, Mathias Gehrig, Yuanyou Li, and Davide Scaramuzza. Time lens: Event-based video frame interpolation. In *Proceedings of the IEEE/CVF conference on computer vision and pattern recognition*, pages 16155–16164, 2021. 2, 7, 8, 9
- [35] Ashish Vaswani, Noam Shazeer, Niki Parmar, Jakob Uszkoreit, Llion Jones, Aidan N Gomez, Łukasz Kaiser, and Illia Polosukhin. Attention is all you need. *Advances in neural information processing systems*, 30, 2017. 6, 8
- [36] Bishan Wang, Jingwei He, Lei Yu, Gui-Song Xia, and Wen Yang. Event enhanced high-quality image recovery. In *Computer Vision–ECCV 2020: 16th European Conference, Glasgow, UK, August 23–28, 2020, Proceedings, Part XIII 16*, pages 155–171. Springer, 2020. 2, 3, 5, 7, 8
- [37] Wenhai Wang, Jifeng Dai, Zhe Chen, Zhenhang Huang, Zhiqi Li, Xizhou Zhu, Xiaowei Hu, Tong Lu, Lewei Lu, Hongsheng Li, et al. Internimage: Exploring large-scale vision foundation models with deformable convolutions. *arXiv preprint arXiv:2211.05778*, 2022. 5
- [38] Zhixiang Wang, Xiang Ji, Jia-Bin Huang, Shin’ichi Satoh, Xiao Zhou, and Yinqiang Zheng. Neural global shutter: Learn to restore video from a rolling shutter camera with global reset feature. In *Proceedings of the IEEE/CVF Conference on Computer Vision and Pattern Recognition*, pages 17794–17803, 2022. 3
- [39] Zhou Wang, Alan C Bovik, Hamid R Sheikh, and Eero P Simoncelli. Image quality assessment: from error visibility to structural similarity. *IEEE transactions on image processing*, 13(4):600–612, 2004. 7
- [40] Zirui Wang, Shangzhe Wu, Weidi Xie, Min Chen, and Victor Adrian Prisacariu. Nerf-: Neural radiance fields without known camera parameters. *arXiv preprint arXiv:2102.07064*, 2021. 3, 6
- [41] Fang Xu, Lei Yu, Bishan Wang, Wen Yang, Gui-Song Xia, Xu Jia, Zhendong Qiao, and Jianzhuang Liu. Motion deblurring with real events. In *Proceedings of the IEEE/CVF International Conference on Computer Vision*, pages 2583–2592, 2021. 3
- [42] Kaihao Zhang, Wenhan Luo, Yiran Zhong, Lin Ma, Bjorn Stenger, Wei Liu, and Hongdong Li. Deblurring by realistic blurring. In *Proceedings of the IEEE/CVF Conference on Computer Vision and Pattern Recognition*, pages 2737–2746, 2020. 4
- [43] Xiang Zhang and Lei Yu. Unifying motion deblurring and frame interpolation with events. In *Proceedings of the IEEE/CVF Conference on Computer Vision and Pattern Recognition*, pages 17765–17774, 2022. 3, 6
- [44] Zhihang Zhong, Yinqiang Zheng, and Imari Sato. Towards rolling shutter correction and deblurring in dynamic scenes. In *Proceedings of the IEEE/CVF Conference on Computer Vision and Pattern Recognition*, pages 9219–9228, 2021. 1, 2, 3, 7, 8
- [45] Xinyu Zhou, Peiqi Duan, Yi Ma, and Boxin Shi. Evunroll: Neuromorphic events based rolling shutter image correction. In *Proceedings of the IEEE/CVF Conference on Computer Vision and Pattern Recognition*, pages 17775–17784, 2022. 1, 2, 3, 7, 8, 9
- [46] Alex Zihao Zhu, Liangzhe Yuan, Kenneth Chaney, and Kostas Daniilidis. Unsupervised event-based learning of optical flow, depth, and egomotion. In *Proceedings of the IEEE/CVF Conference on Computer Vision and Pattern Recognition*, pages 989–997, 2019. 5